IEICE TRANS. ELECTRON., VOL.E102–C, NO.1 JANUARY 2019

PAPER Special Section on Recent Progress in Electromagnetic Theory and Its Application

Kirchhoff Approximation Analysis of Plane Wave Scattering by Conducting Thick Slits

Khanh Nam NGUYEN[†a)], ***Student Member and*** **Hiroshi SHIRAI**[†b)], ***Fellow***

SUMMARY Kirchhoff approximation (KA) method has been applied for ray-mode conversion to analyze the plane wave scattering by conducting thick slits. The scattering fields can be considered as field radiations from equivalent magnetic current sources assumed by closing the aperture of the slit. The obtained results are compared with those of other methods to validate the accuracy of the proposed formulation in different conditions of slit dimension.

key words: *kirchhoff approximation, plane wave scattering, conducting thick slit*

1. Introduction

Developing accurate propagation prediction models for outdoor-indoor communication environments has been paid attention in parallel with the increase of wireless applications. Such models should be analyzed on a practical condition that a particular propagation path may be through a building window, since the concrete walls block the intercommunication by weakening the signal, especially as the frequency increases. Consequently, the study of the electromagnetic wave scattering by a window aperture on the building wall becomes an important practical situation. The plane wave diffraction by a thick slit perforated on a conducting screen can be a canonical problem for this research.

Many authors have approached this aperture scattering problem by applying various calculation methods. Morse and Rubinstein utilize an eigenfunction expansion solution in terms of Mathieu functions [1], while Nomura and Katsura use Kobayashi Potential (KP) method with Weber-Schafheitlin discontinuous integrals [2] to analyze the scattering characteristic by a slit on an infinitely thin screen. KP method is also believed to be effective when solving the thick conducting slits [3], [4] and hole [5]. These cases are more complicated than the thin cases. Wiener-Hopf and generalized matrix technique [6], and Fourier transform technique [7], [8] may also be applied for the thick cases. Nevertheless, the above results have mainly considered relatively narrow slit apertures.

According to the practical situation of radio wave propagation between the inside and outside of the building through windows, the scattering analysis should be focused on the window whose dimension is comparably large with respect to the wavelength. That leads to the study of wide slit rather than narrow one. The high frequency asymptotic methods, such as Geometry Theory of Diffraction (GTD) [9]–[12] and the Kirchhoff approximation (KA) [13], seem to be more effective, in the large aperture circumstance, than eigenfunction expansion methods [2]–[5].

In the previous investigation by GTD [10]–[12], the formulation can be done by using edge diffracted waves excited at the aperture edges with the aid of the ray-mode conversion technique. It has been found that the GTD method exhibits pretty accurate results even for small aperture cases, when one includes the multiple edge diffraction effects. However, the GTD formulation meets a difficulty in derivation of suitable coefficients for the corner or dielectric wedge diffraction cases. Accordingly, it is not clear yet to extend the GTD analysis for the three dimensional cases like a diffraction by a square window aperture. This deficiency of GTD gives us a good motivation for an application of the KA which can be easily extended to practical three dimensional cases. It has already been known that the KA method is effective for high frequency scattering analysis, but the accuracy of the KA formulation is, in general, inferior to the one by GTD [14], [15]. Therefore, we shall study on the accuracy of KA formulation here by applying to the plane wave scattering from a two dimensional conducting thick slit to which other reference solutions are available, before applying to the practical three dimensional problems.

In the following Sect. 2, we first use the KA method to formulate the scattering field. The equivalent magnetic currents on the virtually closed apertures are used to derive the scattering far field at the upper and lower regions of the screen. Scattering feature is also considered when the slit becomes infinitely thin for which a simpler solution is possible. Numerical calculations and discussion are carried out, and the accuracy of presented method is evaluated by comparison with the reference solutions in Sect. 3. Some concluding remarks are made in Sect. 4.

The time-harmonic factor $e^{-i\omega t}$ is assumed and suppressed throughout the text.

2. Formulation

As illustrated in Fig. 1, a plane wave with a unit amplitude:

$$\phi_y^i = e^{-ik(x\cos\theta_0 + z\sin\theta_0)} \tag{1}$$

impinges upon a slit perforated on an infinitely long perfectly conducting thick screen with incident angle θ_0. The

Manuscript received April 10, 2018.
Manuscript revised July 26, 2018.

[†]The authors are with the Graduate School of Science and Engineering, Chuo University, Tokyo, 112–8551 Japan.
a) E-mail: namkhanh@shirai.elect.chuo-u.ac.jp
b) E-mail: shirai@m.ieice.org

DOI: 10.1587/transele.E102.C.12

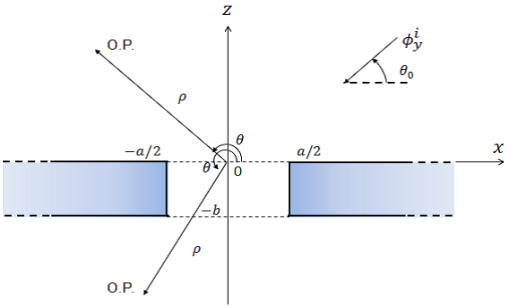

Fig. 1 Geometry of the problem.

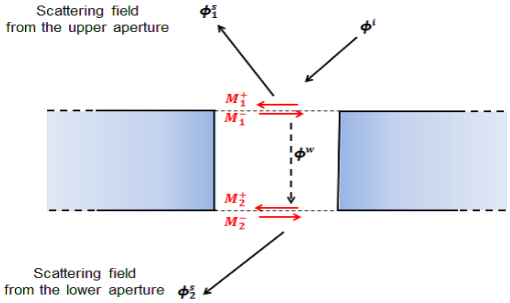

Fig. 2 Scattering fields at each region may be considered as radiations from the equivalent sources at the apertures.

width and thickness of the slit are a and b, respectively, and k is the free space wavenumber. ϕ_y^i represents for $E_y^i(H_y^i)$ for E(H) polarization. In order to determine the scattering contributions ϕ_y^s, the KA method is utilized here. Consequently, the scattering fields are obtained as radiations from the equivalent magnetic current sources on the virtually closed apertures. By doing so, there exists a reflected field $\boldsymbol{\phi}^r$ due to the reflection from the screen's surface at $z = 0$ in the upper half-space ($z > 0$) as

$$\phi_y^r = \begin{pmatrix} E_y^r \\ H_y^r \end{pmatrix} = \mp e^{-ik(x\cos\theta_0 - z\sin\theta_0)}, \tag{2}$$

for E and H polarizations. This contribution will be omitted in the following analysis.

2.1 E Polarization

2.1.1 Scattering in the Upper Region ($z > 0$)

The equivalent magnetic current sources $\boldsymbol{M}_1^{\pm}$ on the closed upper aperture as in Fig. 2 may be obtained from the incident electric field as

$$\begin{aligned} \boldsymbol{M}_1^{\pm}(x, z = 0_{\pm}) &= E_y^i \hat{\boldsymbol{y}}\big|_{z=0} \times (\pm\hat{\boldsymbol{z}}) \\ &= \pm e^{-ikx\cos\theta_0}\hat{\boldsymbol{x}}, \quad \left(|x| < \frac{a}{2}\right), \end{aligned} \tag{3}$$

where '$\hat{}$' denotes the corresponding unit vector. Then the scattering E_{1y}^s field from the upper aperture can be expressed in terms of the equivalent magnetic current $\boldsymbol{M}_1^+$ on the upper side of the upper aperture as [15]

$$E_{1y}^s = \int_{-a/2}^{a/2} M_{1x}^+(x')\frac{\partial}{\partial z'}G(x, z; x', z' = 0_+)dx', \tag{4}$$

where G is the two dimensional half space Green's function considering the imaging effect of the magnetic current on the boundary

$$\begin{aligned} G(x, z; x', z') &= \frac{i}{2}\mathrm{H}_0^{(1)}(k\sqrt{(x-x')^2 + (z-z')^2}) \\ &= \frac{i}{2\pi}\int_{-\infty}^{\infty} \frac{e^{i\eta(x-x') + i\sqrt{k^2-\eta^2}|z-z'|}}{\sqrt{k^2-\eta^2}}d\eta. \end{aligned} \tag{5}$$

Here, $\mathrm{H}_0^{(1)}(\chi)$ is the zero-th order Hankel function of the first kind. Substituting Eq. (5) into Eq. (4) and evaluating the integral with respect to x' variable first. Then one gets

$$\begin{aligned} E_{1y}^s = \frac{i}{2\pi}\int_{-\infty}^{\infty} e^{i\sqrt{k^2-\eta^2}z} \\ \cdot \frac{e^{-ik(a/2)\cos\theta_0 + i\eta(x-a/2)} - e^{ik(a/2)\cos\theta_0 + i\eta(x+a/2)}}{(k\cos\theta_0 + \eta)}d\eta. \end{aligned} \tag{6}$$

Since the above integral can not be evaluated in a closed form, the saddle point method may be applied to evaluate the integral for a large k. One can derive the scattering far field in the upper half space ($z > 0$) as (see Appendix A)

$$E_{1y}^s = \frac{-4i\sin\theta\sin\left[\frac{ka}{2}(\cos\theta_0 + \cos\theta)\right]}{\cos\theta_0 + \cos\theta}C(k\rho), \tag{7}$$

$$C(k\rho) = \sqrt{\frac{1}{8\pi k\rho}}e^{ik\rho + i\pi/4}. \tag{8}$$

2.1.2 Modal Excitation Inside the Slit

A part of the incident plane wave penetrates through the slit aperture and this field eventually leads to the scattering field in the lower half space. In the previous study by GTD [10]–[12], the field in the slit has been considered to be excited by the aperture edges ($x = \pm a/2, z = 0$), and the exciting waveguide modes have been derived from the ray-mode conversion method. In this investigation, however, a different ray-mode conversion has been introduced. The modal excitation is given by equivalent magnetic source $\boldsymbol{M}_1^-$ on the closed aperture. The excited field $\boldsymbol{E}^w$ inside a semi-infinitely long ($b \to \infty$) parallel plane waveguide may be expressed as

$$E_y^w = \int_{-a/2}^{a/2} M_{1x}^-(x')\frac{\partial}{\partial z'}G^w(x, z; x', z' = 0_-)dx', \tag{9}$$

where G^w is the Green's function for a parallel plane waveguide considering the imaging effect for the metal closure at the aperture, namely

$$\begin{aligned} G^w(x, z; x', z') = \sum_{m=1}^{\infty}\frac{2i}{a\zeta_m}\sin\frac{m\pi}{a}\left(x + \frac{a}{2}\right) \\ \cdot \sin\frac{m\pi}{a}\left(x' + \frac{a}{2}\right)e^{i\zeta_m|z-z'|}, \end{aligned} \tag{10}$$

and ζ_m denotes the wave number in z-direction as

$$\zeta_m = \sqrt{k^2 - \left(\frac{m\pi}{a}\right)^2}. \tag{11}$$

The field propagating downward inside the slit may be derived as

$$E_y^w = \sum_{m=1}^{\infty} F_m \sin\frac{m\pi}{a}\left(x + \frac{a}{2}\right) e^{-i\zeta_m z}. \tag{12}$$

Here, F_m is the excitation coefficient of the $\mathrm{TE_m}$ waveguide modal field. F_m can be calculated by integrating the equivalent source $\boldsymbol{M}_1^-$ over the aperture ($|x| \le a/2, z = 0_-$), one gets

$$F_m = -\frac{2m\pi}{[(m\pi)^2 - (ka\cos\theta_0)^2]} \cdot \left[(-1)^m e^{(-ika\cos\theta_0)/2} - e^{(ika\cos\theta_0)/2}\right]. \tag{13}$$

The internal waveguide field $\boldsymbol{E}^w$ propagates down to the lower aperture ($z = -b$) and excites there scattering field $\boldsymbol{E}_2^s$ to the lower half space ($z < -b$), and the modal reflection ($z > -b$). These scattering fields are again calculated from the equivalent magnetic currents $\boldsymbol{M}_2^{\pm}$ on the closed aperture at $z = -b$, as in Fig. 2. The equivalent magnetic current $\boldsymbol{M}_2^{\pm}$ can be found from

$$\boldsymbol{M}_2^{\pm}(x, z = -b_{\pm}) = E_y^w \hat{\boldsymbol{y}}\big|_{z=-b} \times (\pm\hat{\boldsymbol{z}}) = \pm \sum_{m=1}^{\infty} F_m \sin\frac{m\pi}{a}\left(x + \frac{a}{2}\right) e^{i\zeta_m b}\hat{\boldsymbol{x}}, \quad \left(|x| < \frac{a}{2}\right). \tag{14}$$

For modal reflection, one may use the similar formula in Eq. (9) with M_{2x}^+ in Eq. (14). After some calculations, one finds that the modal coefficients obtained from the equivalent magnetic current M_{2x}^+ become unit values which cancel the reflection coefficients (-1) of the waveguide modes by closing the lower aperture. Consequently, there is no reflection at all from the lower aperture by the Kirchhoff approximation. In our previous formulation by GTD [10]–[12] where more rigorous ray-mode conversion method using Poisson summation formula is used, and there are some modal reflections and coupling even at the lower aperture, while these effects are weak. However in our present investigation, a different ray-mode conversion is introduced through the equivalent currents on the aperture. Accordingly, in this formulation, the scattering field in the upper half region ($z > 0$) E_y^s is approximately given by E_y^r in Eq. (2) plus E_{1y}^s in Eq. (7), and no further modal re-radiation fields.

2.1.3 Scattering in the Lower Region ($z < -b$)

The radiation field $\boldsymbol{E}_2^s$ in the lower half-space can be derived from the equivalent source $\boldsymbol{M}_2^-$ in Eq. (14) like the primary scattering field $\boldsymbol{E}_1^s$ in Sect. 2.1.1. $\boldsymbol{E}_2^s$ becomes

$$E_{2y}^s = \int_{-a/2}^{a/2} M_{2x}^-(x')\frac{\partial}{\partial z'} G(x, z; x', z' = -b_-)dx'. \tag{15}$$

Once again, the integral in Eq. (15) can be evaluated using the saddle point method. One gets the scattering field E_{2y}^s for $\theta > \pi$ as

$$E_{2y}^s = 2ka\sin\theta\, C(k\rho) \sum_{m=1}^{\infty} F_m \frac{m\pi}{(m\pi)^2 - (ka\cos\theta)^2} \cdot \left[(-1)^m e^{(-ika\cos\theta)/2} - e^{(ika\cos\theta)/2}\right] e^{i\zeta_m b}. \tag{16}$$

It may be interesting to derive a special circumstance of an infinitely thin slit, one can take the limit $b \to 0$ in Eq. (16). On the other hand, the lower scattering field in this case $\boldsymbol{E}_2^{ss}$ can be derived directly from $\boldsymbol{M}_1^-$ in Eq. (3) in the similar way of deriving $\boldsymbol{E}_1^s$. One gets for $\theta > \pi$

$$E_{2y}^{ss} = -E_{1y}^s = \frac{4i\sin\theta\sin\left[\frac{ka}{2}(\cos\theta_0 + \cos\theta)\right]}{\cos\theta_0 + \cos\theta} C(k\rho). \tag{17}$$

One observes that E_{2y}^{ss} is symmetric with respect to the conducting surface ($z = 0$). The comparison of results from these two calculations will be shown in Sect. 3.

2.2 H Polarization

Similar derivation can be made for H polarization. We shall show here the main results only without detail derivation.

2.2.1 Scattering in the Upper Region ($z > 0$)

The equivalent magnetic current sources $\boldsymbol{M}_1^{\pm}$ on the closed upper aperture may be obtained from the incident electric field as

$$\boldsymbol{M}_1^{\pm}(x, z = 0_{\pm}) = (E_x^i\hat{\boldsymbol{x}} + E_z^i\hat{\boldsymbol{z}})\big|_{z=0} \times (\pm\hat{\boldsymbol{z}}) = \pm\sqrt{\frac{\mu_0}{\varepsilon_0}}\sin\theta_0 e^{-ikx\cos\theta_0}\hat{\boldsymbol{y}}, \quad \left(|x| < \frac{a}{2}\right), \tag{18}$$

where μ_0 and ε_0 denote the free space permeability and permittivity, respectively. Then scattering field H_{1y}^s from the upper aperture can be expressed in terms of the equivalent magnetic current $\boldsymbol{M}_1^+$ on the upper side of the upper aperture as [15]

$$H_{1y}^s = i\omega\varepsilon_0 \int_{-a/2}^{a/2} M_{1y}^+(x')G(x, z; x', z' = 0_+)dx'. \tag{19}$$

Substituting Eq. (5) into Eq. (19) and evaluating the integral by the saddle point method asymptotically, one can derive the scattering far field in the upper half space ($z > 0$) as

$$H_{1y}^s = \frac{4i\sin\theta_0\sin\left[\frac{ka}{2}(\cos\theta_0 + \cos\theta)\right]}{\cos\theta_0 + \cos\theta} C(k\rho). \tag{20}$$

2.2.2 Modal Excitation Inside the Slit

The field $\boldsymbol{H}^w$ inside a semi-infinitely long ($b \to \infty$) parallel plane waveguide may be derived from the equivalent magnetic source $\boldsymbol{M}_1^-$ in Eq. (18) on the closed aperture as

$$H_y^w = i\omega\varepsilon_0 \int_{-a/2}^{a/2} M_{1y}^-(x')\bar{G}^w(x,z;x',z'=0_-)dx', \quad (21)$$

where $\bar{G}^w$ is, again, the Green's function for parallel plane waveguide considering the imaging effect for the metal closure at the aperture. For this polarization, the Green's function has a different boundary condition at $x = \pm a/2$, and is given by

$$\bar{G}^w(x,z;x',z') = \sum_{m=0}^{\infty} \frac{i\epsilon_m}{a\zeta_m} \cos\frac{m\pi}{a}\left(x+\frac{a}{2}\right) \cdot \cos\frac{m\pi}{a}\left(x'+\frac{a}{2}\right) e^{i\zeta_m|z-z'|}, \quad (22)$$

where $\epsilon_m = \begin{cases} 1, & m=0 \\ 2, & m>0 \end{cases}$. The field propagating downward inside the slit may be derived as

$$H_y^w = \sum_{m=0}^{\infty} \bar{F}_m \cos\frac{m\pi}{a}\left(x+\frac{a}{2}\right) e^{-i\zeta_m z}. \quad (23)$$

Here, the excitation coefficient of the TM_m waveguide modal field $\bar{F}_m$ becomes

$$\bar{F}_m = -\frac{i\epsilon_m k^2 a \sin\theta_0 \cos\theta_0}{\zeta_m[(m\pi)^2 - (ka\cos\theta_0)^2]} \cdot \left[(-1)^m e^{(-ika\cos\theta_0)/2} - e^{(ika\cos\theta_0)/2}\right]. \quad (24)$$

The equivalent magnetic currents $\boldsymbol{M}_2^{\pm}$ on the closed aperture at $z = -b$ are found from

$$\boldsymbol{M}_2^{\pm}(x, z=-b_{\pm}) = (E_x^w\hat{\boldsymbol{x}} + E_z^w\hat{\boldsymbol{z}})\big|_{z=-b} \times (\pm\hat{\boldsymbol{z}})$$
$$= \mp\sum_{m=0}^{\infty} \bar{F}_m \cos\frac{m\pi}{a}\left(x+\frac{a}{2}\right) e^{i\zeta_m b}\hat{\boldsymbol{y}}, \quad \left(|x| < \frac{a}{2}\right). \quad (25)$$

Again, equivalent current M_2^+ yields the radiation field which cancels the reflected modal field due to the postulated metal closure at the aperture $z = -b$. Accordingly, there are no net reflected modes propagating upward for our approximation.

2.2.3 Scattering in the Lower Region ($z < -b$)

The radiation field $\boldsymbol{H}_2^s$ in the lower half-space can be derived from the equivalent source $\boldsymbol{M}_2^-$ in Eq. (25). One gets the scattering far field $\boldsymbol{H}_2^s$ as

$$H_{2y}^s = 2ka\cos\theta\, C(k\rho) \sum_{m=0}^{\infty} \bar{F}_m \frac{-\zeta_m a}{(m\pi)^2 - (ka\cos\theta)^2} \cdot \left[(-1)^m e^{(-ika\cos\theta)/2} - e^{(ika\cos\theta)/2}\right] e^{i\zeta_m b}. \quad (26)$$

For an infinitely thin slit, the lower scattering far field $\boldsymbol{H}_2^{ss}$ can be derived from $\boldsymbol{M}_1^-$ in Eq. (18) in the similar way of deriving $\boldsymbol{H}_1^s$. One gets

$$H_{2y}^{ss} = -H_{1y}^s = \frac{-4i\sin\theta_0 \sin\left[\frac{ka}{2}(\cos\theta_0 + \cos\theta)\right]}{\cos\theta_0 + \cos\theta} C(k\rho). \quad (27)$$

3. Numerical Results and Discussion

The formulas derived in the previous section are now used to obtain some numerical results for the scattering far fields. In the following calculations, a common factor $C(k\rho)$ is omitted, as well as the reflected wave ϕ_y^r.

Figures 3 and 4 show the scattering far field for E and H polarizations, respectively. The aperture widths are set to be $ka = 30, 7$, the screen thickness is $kb = 2$, and the incident angle $\theta_0 = 50°$ is chosen. As can be seen from the figures, the wider the aperture is, the stronger the scattering fields become, especially at the main lobe. More diffraction lobes are constructed due to the interference between the radiation fields excited at the edges at $x = \pm a/2$. For comparison, the figures include the results obtained by the GTD [10], [11] and by the KP method [3]. The GTD is known to be an effective method for high frequency regime for large apertures, while the KP is the eigenfunction expansion method which is effective for small apertures. One observes that the main lobes direct the corresponding reflected and incident shadow boundary directions near $\theta = 130°$ and $230°$. While our results denoted by KA match well with other results at these main lobe directions, one finds some differences in the figures at some side lobes near boundaries. This is due to the fact that KA solution does not satisfy the boundary con-

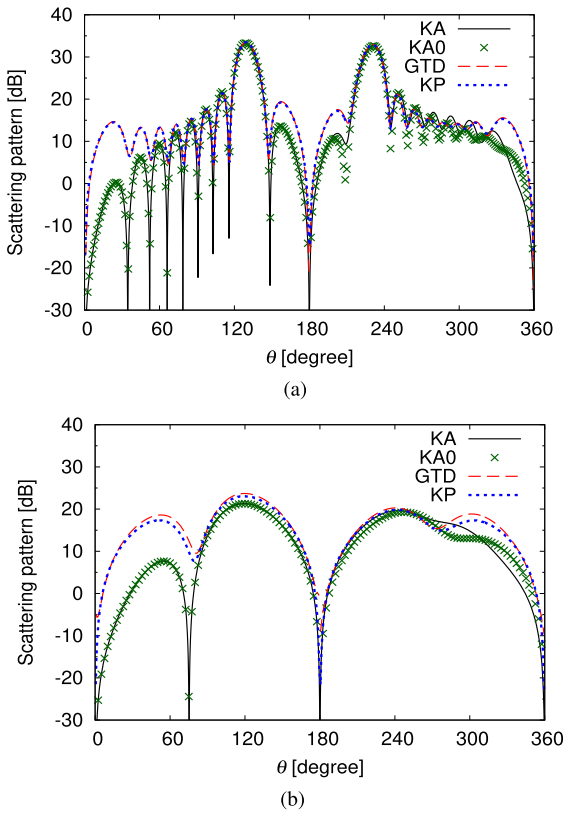

Fig. 3 Comparison of the far-field patterns in dB (width variation) of KA, KP and GTD methods. E polarization $\theta_0 = 50°$, $kb = 2$. (a) $ka = 30$. (b) $ka = 7$.

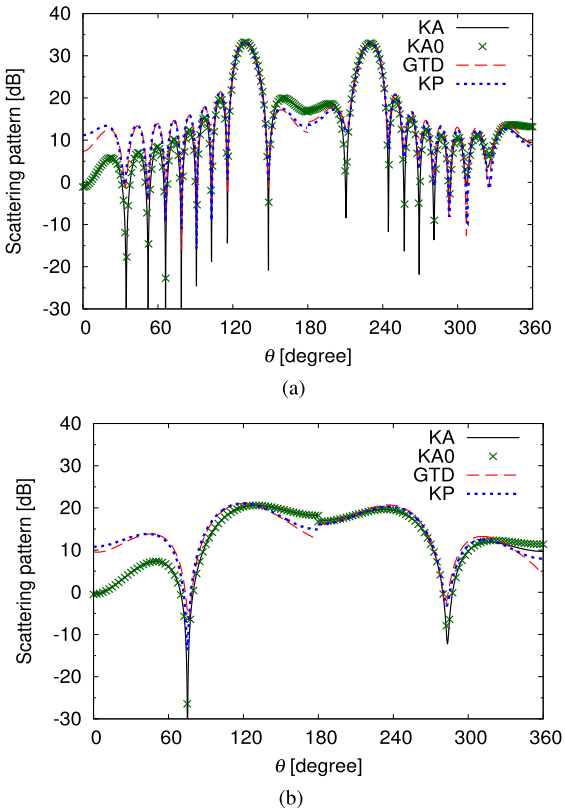

Fig. 4 Comparison of the far-field patterns in dB (width variation) of KA, KP and GTD methods. H polarization $\theta_0 = 50°$, $kb = 2$. (a) $ka = 30$. (b) $ka = 7$.

dition [15], and the multiple edge diffraction terms cannot be considered.

When the current KA formulation is compared with those by GTD [10],[11], main difference maybe found in the modal re-radiation field. Since the KA approximation yields no waveguide modal reflections and couplings at the open end, modal re-radiation occurs only once at the lower aperture. Accordingly, one does not need to solve the matrix equation for the successive modal re-radiation fields [10]. Then one can expect fast calculation. By comparing the CPU time for numerical evaluation, the present method is 1.5 times faster than the previous GTD formulation [10]. This is effective for wide aperture cases, since many waveguide modes will be excited in the slit, and the coupling between them become involved to compute.

For transmitted region ($\theta > \pi$), one sees from the previous section that the scattering fields are given by a summation of the modal re-radiation fields as in Eqs. (16) and (26). The main transmitted lobe is made by the significant modes whose propagation angles are in the vicinity of the incident angle θ_0, and these modal excitation coefficients become large [13] for rather thin slit cases. In order to see the effect of the evanescent modal re-radiation, our KA results are obtained by including first three evanescent modal re-radiations, whereas results denoted as KA0 by cross symbols are calculated without the evanescent modal

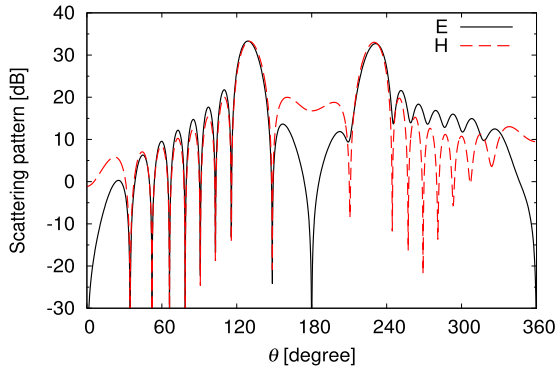

Fig. 5 Comparison of E and H polarizations of far-field patterns in dB. $\theta_0 = 50°$, $ka = 30$, $kb = 2$.

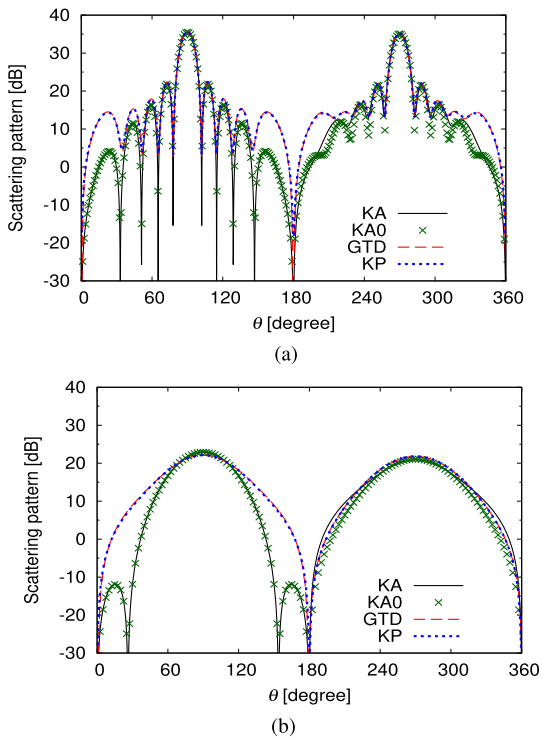

Fig. 6 Comparison of the far-field patterns of KA, KP and GTD methods in dB. $kb = 2$ and $\theta_0 = 90°$. E polarization (a) $ka = 30$. (b) $ka = 7$.

contribution. One observes a small difference between them at $250° < \theta < 360°$ especially for a small aperture case ($ka = 7$). Of course, there are no differences in the upper region ($z > 0$), since no modal re-radiation appears in our KA formulation as mentioned before.

Figure 5 shows the scattering pattern difference between E and H polarizations. The main feature of the scattering pattern is almost the same between E and H polarizations. However, the difference occurs at the boundary direction at $\theta = 0°, 180°, 360°$ due to the boundary conditions.

The scattering pattern for the normal incidence case ($\theta_0 = 90°$) are shown in Fig. 6 for E polarization and Fig. 7 for H polarization, respectively. Symmetric pattern with respect to the normal (z) axis is observed for all plots. The

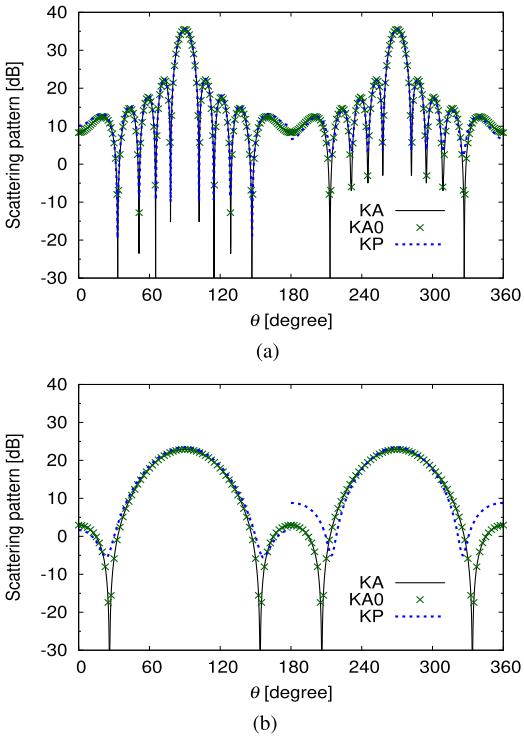

Fig. 7 Comparison of the far-field patterns of KA and KP methods in dB. $kb = 2$ and $\theta_0 = 90°$. H polarization (a) $ka = 30$. (b) $ka = 7$.

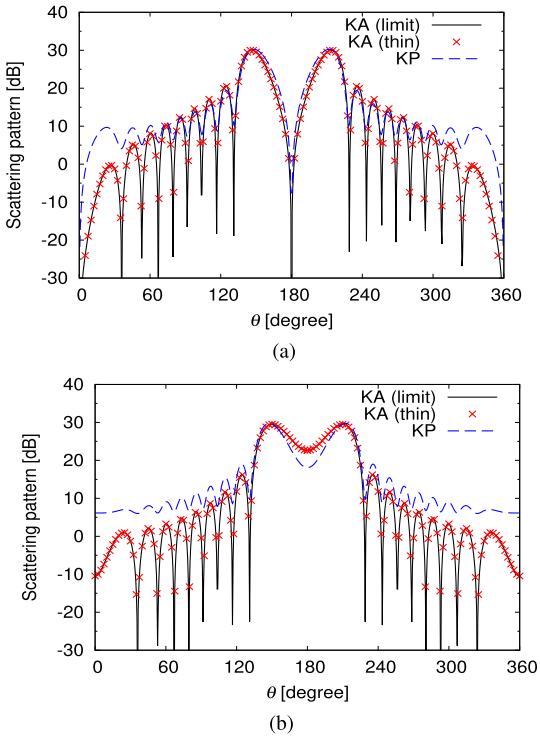

Fig. 8 Comparison of the far-field patterns in thin slit case. $\theta_0 = 30°$, $ka = 30$, $kb \to 0$. (a) E polarization. (b) H polarization

error of KA formulation at the side-lobe direction is somewhat bigger for E polarization than that for H polarization.

Let us now discuss the thin slit case. In our formulation, the thickness was assumed on the premise and the field ϕ_y^w inside the slit has been represented by the parallel plane waveguide modes, as in Eqs. (12) and (23). It is found that our formulation for the lower region has a limit value for taking a limit of an infinitely thin case ($b \to 0$), while the direct formulation for this case is possible by considering the equivalent current $\boldsymbol{M}_1^{\pm}$ only. Figure 8 shows the difference between the limit cases in Eqs. (16) and (26) and the direct formulation cases in Eqs. (17) and (27). Both results are indistinguishable. The scattering patterns in this circumstance calculated by KA method are compared with those of KP method. One observes that the scattering patterns become symmetric with respect to the boundary (x) direction.

Figure 9 shows the case for $ka = 50$ of different slit thickness. Again, KA solution predicts well for main diffraction beam directions. When the aperture becomes wider, the side lobe levels get lower. Accordingly, one does not need to worry about the KA accuracy if one estimates the main feature of the diffraction pattern. Figures 10 and 11 show the normalized scattering pattern changes by the thickness of the slit. All figures are calculated for $ka = 50$ by our KA method for both E and H polarizations. Figure 10 shows the pattern changes from an infinitely thin case to the finite thin case. In the upper region ($z > 0$), the patterns do not change, since the primary scattering fields excited by $\boldsymbol{M}_1^{+}$ contain no information on the slit's thickness. On the other

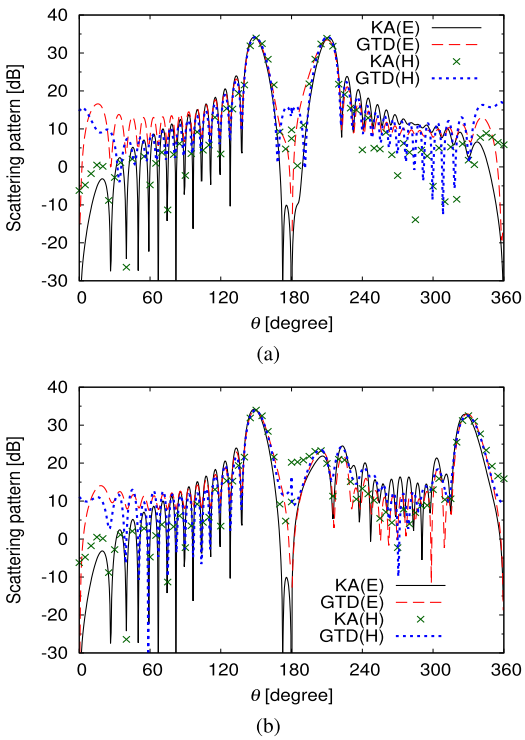

Fig. 9 Comparison of the far-field patterns of KA and GTD methods. $\theta_0 = 30°$, $ka = 50$. (a) $kb = 1$ (thin case). (b) $kb = 50/\sqrt{3}$ (thick case).

hand, the symmetric patterns with respect to the boundary (x) direction for an infinitely thin case ($kb = 0$) deteriorate as the thickness becomes a finite value. This effect occurs

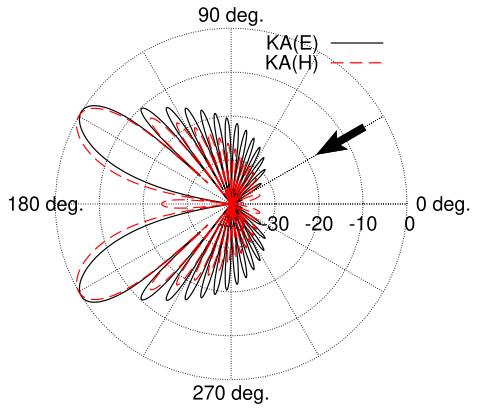

(a)

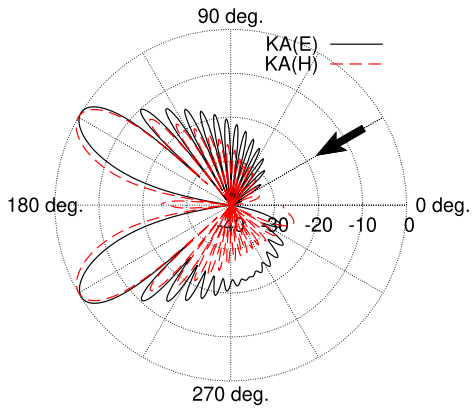

(b)

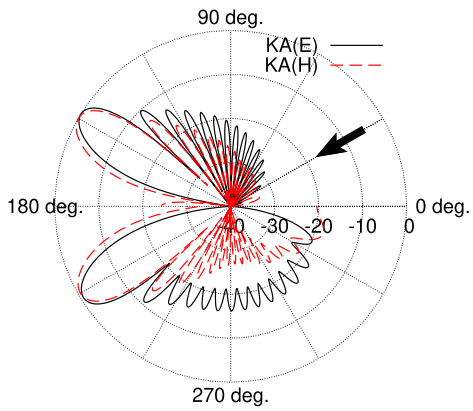

(c)

Fig. 10 Change of normalized far-field patterns from thin slits in dB. $\theta_0 = 30°$, $ka = 50$. (a) $kb = 0$. (b) $kb = 1.0$. (c) $kb = 2.5$.

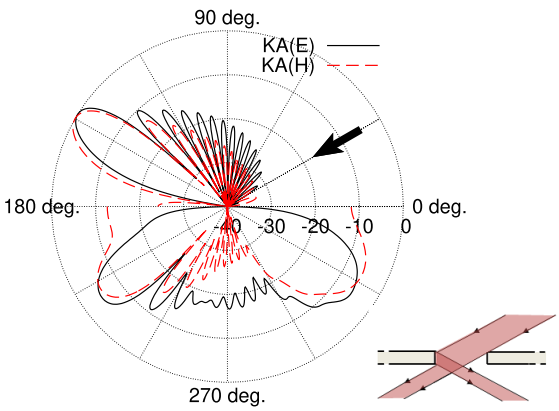

(a)

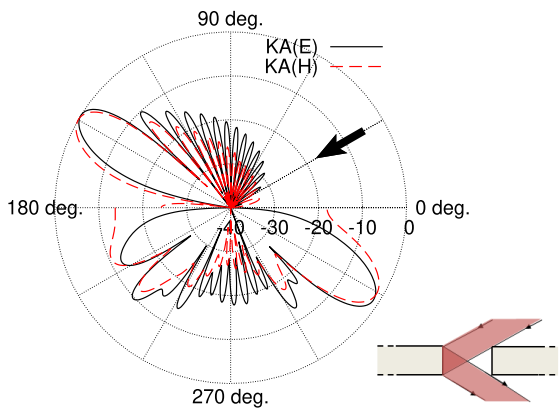

(b)

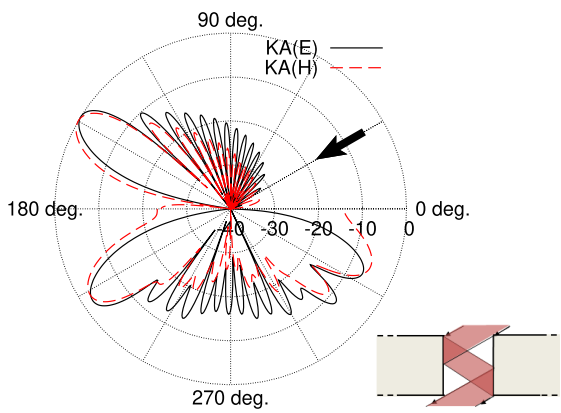

(c)

Fig. 11 Change of normalized far-field patterns from thick slits in dB. $\theta_0 = 30°$, $ka = 50$. (a) $kb = 25/\sqrt{3}$. (b) $kb = 50/\sqrt{3}$. (c) $kb = 100/\sqrt{3}$.

even for relatively thin case in Fig. 10(b) for $b/a = 0.02$, and this thickness effect seems to be more influential for E polarization.

Figure 11 shows the pattern changes for pretty thick cases. Three thickness cases are chosen here to show the incident beam splitting. Because of the slit's thickness, incident plane wave experiences the reflection at the internal slit wall. Accordingly, the geometrical optic (GO) beam yields a splitting. A half splitting can be seen in Fig. 11(a) for $kb = 25/\sqrt{3}$, and the scattering pattern in the lower region becomes roughly symmetric with respect to the normal (z) axis. The total GO beam reflection occurs in Fig. 11(b) for $kb = 50/\sqrt{3}$, and the GO beam propagation due to the double bouncing can be observed Fig. 11(c) for $kb = 100/\sqrt{3}$. While the incident plane wave in the slit's aperture is converted into the waveguide modes, the original GO beam feature of reflection is kept by modal re-radiation field correctly.

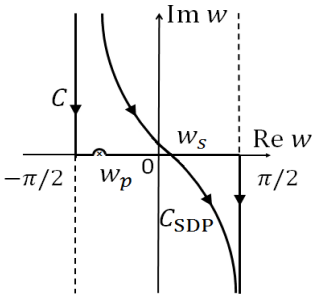

Fig. 12 Integration contour C and C_{SDP} for I_1 in the complex angular w plane

4. Conclusion

In this study, plane wave scattering by conducting thick slits has been formulated by KA method. The scattering field can be obtained by the radiation from the equivalent magnetic currents on the closed aperture of the slit. For the transmitted field in the lower region ($z < 0$), the penetrating fields in the slit region are expressed first by parallel plane waveguide modes, then these fields are again converted into the equivalent currents to excite the modal re-radiation fields. The comparison with GTD and KP methods shows the validity of our formulation, especially for the large aperture cases in both thin and thick cases. Especially the KA formulation can predict well for main diffraction beam directions by a shorter calculation time than the previous GTD formulation. Since our KA method can straightforwardly be extended for the three dimensional cases, one could expect that more realistic problems such as the scattering by a large square window can be analyzed efficiently within a minimal error. These aspects are now under the investigation.

Acknowledgments

A part of this study is supported by a Scientific Research Grant In Aide (15K06083, 2015) from the Japan Society for the Promotion of Science, Japan, and Chuo University Personal Research Grant.

References

[1] P.M. Morse and P.J. Rubenstein, "The diffraction of waves by ribbons and by slits," Phys. Rev., vol.54, no.11, pp.895–898, Dec. 1938.
[2] Y. Nomura and S. Katsura, "Diffraction of electromagnetic waves by ribbon and slit. I," J. Phys. Soc. Jpn., vol.12, no.2, pp.190–200, 1957.
[3] K. Hongo, "Diffraction of electromagnetic plane wave by infinite slit perforated in a conducting screen with finite thickness," Trans. IECE, vol.54B, no.7, pp.419–425, July 1971 (in Japanese).
[4] K. Hongo and G. Ishii, "Diffraction of an electromagnetic plane wave by a thick slit," IEEE Trans. Antennas Propag., vol.26, no.3, pp.494–499, May 1978.
[5] H. Serizawa, "Diffraction of a plane wave by a rectangular hole in a thick conducting screen," Proc. 2015 European Conference on Antennas and Propagation, pp.1–5, April 2015.
[6] S. Kashyap and M. Hamid, "Diffraction characteristics of a slit in a thick conducting screen," IEEE Trans. Antennas and Propag., vol.19, no.4, pp.499–507, July 1971.
[7] S.H. Kang, H.J. Eom, and T.J. Park, "TM scattering from a slit in a thick conducting screen: Revisited," IEEE Trans. Microw. Theory Techn., vol.41, no.5, pp.895–899, May 1993.
[8] T.J. Park, S.H. Kang, and H.J. Eom, "TE scattering from a slit in a thick conducting screen: Revisited," IEEE Trans. Antennas and Propag., vol.42, no.1, pp.112–114, Jan. 1994.
[9] S.N. Karp and A. Russek, "Diffraction by a wide slit," J. Appl. Phys., vol.27, no.8, pp.886–894, Aug. 1956.
[10] H. Shirai and R. Sato, "High frequency ray-mode coupling analysis of plane wave diffraction by a wide and thick slit on a conducting screen," IEICE Trans. Electron., vol.E95-C, no.1, pp.10–15, Jan. 2012.
[11] H. Shirai, M. Shimizu, and R. Sato, "Hybrid ray-mode analysis of E-polarized plane wave diffraction by a thick slit," IEEE Trans. Antennas and Propag., vol.64, no.11, pp.4828–4835, Nov. 2016.
[12] M. Shimizu, H. Shirai and R. Sato, "Electromagnetic scattering analysis by a window model on a building wall," IEICE Trans. Electron., vol.J100-C, no.7, pp.295–301, July 2017 (in Japanese).
[13] H. Shirai and L.B. Felsen, "Rays, modes and beams for plane wave coupling into a wide open-ended parallel-plane waveguide," Wave motion, vol.9, no.4, pp.301–317, July 1987.
[14] L. Diaz and T. Milligam, Antenna Engineering Using Physical Optics, Artech House, Norwood, MA, USA, 1996.
[15] H. Shirai, Geometrical Theory of Diffraction, Corona Publishing Co., Ltd., 2015 (in Japanese).

Appendix A: Derivation of Eq. (7)

Equation (6) may be separated into I_1 and I_2 as

$$I_{1,2} = \pm\frac{i}{2\pi}\int_{-\infty}^{\infty}\frac{e^{\mp ik(a/2)\cos\theta_0 + i\eta(x\mp a/2)+i\sqrt{k^2-\eta^2}z}}{(k\cos\theta_0+\eta)}d\eta. \quad (\mathrm{A}\cdot 1)$$

Introducing the cylindrical coordinates $x \mp a/2 = \rho_\pm\cos\theta_\pm$, $z = \rho_\pm\sin\theta_\pm$ and the transformation $\eta = k\sin w$, the integral $I_{1,2}$ can be written as

$$I_{1,2} = \pm\frac{i}{2\pi}\int_C \frac{e^{\mp ik(a/2)\cos\theta_0 + ik\rho_\pm\sin(w+\theta_\pm)}}{\cos\theta_0+\sin w}\cos w\, dw, \quad (\mathrm{A}\cdot 2)$$

where the integration contour C is shown in Fig. 12 in the complex angular w plane. There is a pole singularity w_p at $w_p = -\arcsin(\cos\theta_0)$ and a saddle point w_s at $w_s = \pi/2-\theta_\pm$. When one deforms the integration contour C to the steepest descent path C_{SDP}, the integral can be evaluated asymptotically by [15]

$$\begin{aligned} I_{1,2} \;=\; & \pm\frac{2\sin\theta_\pm}{\cos\theta_0+\cos\theta_\pm}e^{\mp ik(a/2)\cos\theta_0}C(k\rho_\pm) \\ & \pm e^{-ik(x\cos\theta_0 - z\sin\theta_0)}U(\theta_\pm+\theta_0-\pi), \end{aligned} \quad (\mathrm{A}\cdot 3)$$

where $U(\chi) = \begin{cases}1, & \chi>0\\ 0, & \chi<0\end{cases}$ is a unit step function. The second term in Eq. (A·3) represents the residue contribution due to the pole w_p. If the observation point is far from the origin, one may approximate as $\rho_\pm \sim \rho \mp (a/2)\cos\theta$ and $\theta_\pm \sim \theta$, then summing up the first (the saddle point contribution) terms of I_1 and I_2 yields Eq. (7). The second (the pole contribution) terms of I_1 and I_2 cancel each other to yield null contribution.

Khanh Nam Nguyen received the B.E. in Telecommunication Engineering from Hanoi University of Science and Technology, and the M.E. degree in Electrical, Electronic, and Communication Engineering from Chuo University, Japan, in 2014 and 2018, respectively. He is now a Ph.D. student at Chuo University, Japan. His current research interest is electromagnetic scattering. Mr. Nguyen is a student member of the IEEE.

Hiroshi Shirai received the B.E. and the M.E. degrees in Electrical Engineering from Shizuoka University, Japan, in 1980 and 1982, respectively, and the Ph.D. degree from Polytechnic University (presently re-named as Tandon School of Engineering, New York University), New York in 1986. He was a Research Fellow, then a Postdoctoral Scientist until March 1987 in Polytechnic University. Since April 1987, he has been with Chuo University, Tokyo, Japan, where he is currently a Director of International Center and a Professor. He has been serving as a committee member of various technical societies and international meetings. He is now an Editor in Chief of IEICE Transaction on Fundamentals, and an Editorial Advisory member of IEICE Fundamentals Review. He received the R.W.P. King Best Paper Award from the Antennas and Propagation Society of the IEEE in 1987. His current research interests include wave propagation and diffraction in time harmonic and transient domains. Dr. Shirai is a senior member of the IEEE, and a member of Sigma Xi, the IEE of Japan.